CHAPTER IX
GEL ELECTROLYTE OF POLYMETHYL ARCYLATE AND CLAY AEROGEL FOR DYE-SENSITIZED SOLAR CELLS

9.1 Abstract

A composite aerogel of polymethyl acrylate coating on purified Na-bentonite was successfully used to prepare gel electrolyte for dye-sensitized solar cell. The polymethyl acrylate (PMA) and purified Na-bentonite ratio of composite aerogel and the composite content in electrolyte were determined to search for a weak gel with high diffusion conductivity of redox electrolyte in gel electrolyte. The 10 wt.% PMA90 is the optimum and its photovoltaic properties, J_{sc}, V_{oc}, FF, and %η is 655 V, 7.8 mA/cm^2, 0.67, and 3.41%, respectively.

Keywords: Titanium dioxide; polymer/clay aerogel; Gel electrolyte; Diffusion conductivity; Rheological properties; Photovoltaic properties

9.2 Introduction

Sealing is one of the main problem of DSSCs. A nanosized SiO_2 powder and Al_2O_3 have been used to form gel with liquid electrolyte since in the study of Kay (1994). With about 10 wt.% nanosized SiO_2, gel matrix does not influence the ion diffusion in the electrolyte. Park *et al.* (2008) reported that 20 wt.% synthetic laponite with 100 nm of platelet size in MPN base electrolyte improved J_{sc} by 2.3 mA/cm^2. They attributed this improvement to light scattering effect of clay particle in electrolyte. In addition, some studies found that the addition of small amount of modified-surface clay (0.5 wt.%) (Lai *et al.*, 2009) or mica (3 wt.%) (Lai *et al.*, 2010) could enhance ion exchange mechanism of PVDF-HFP gel electrolyte, which led to an increase in J_{sc} about 4 to 5 mA/cm^2. Interestingly, Tu *et al.* (2008) reported that poly (n-isopropylacrylamide) (PNIPAAm) and its nanocomposite with exfoliated montmorillonite (MMT) prepared by soap-free emulsion polymerization

provided higher J_{sc} than that of PNIPAAm gel electrolyte by 5.32 mA/cm^3. The contribution of this photocurrent probably resulted from the ion diffusion facilitation of MMT particles. This is perhaps the effect of ion conducting pathways of the MMT surface, which was explained in the same way like the proton conducting pathways of hydrophilic metal oxides in the composite membrane of direct methanol fuel cell (Sasajima *et al.*, 2008). In DSSC, the electron exchange reaction takes place on the SiO_2 surface as the report of Berginc *et al.*, 2008 or the Grotthus-type exchange mechanism as described in Zakeeruddin and Grätzel, 2009.

The soap-free emulsion polymerization was used to synthesize polymethyl acrylate (Chen and Sajjadi, 2009; Tu *et al.*, 2008). The clay aerogel/PMA composite was prepared form the mixture of PMA latex and swollen purified Na-bentonite frozen and dried under vacuum (Pojanavaraphan *et al.*, 2010). Polymethyl acrylate on Na-bentonite aerogel was utilized as a gelator for liquid electrolyte in DSSCs. The polymer: clay ratio and composite content in liquid electrolyte were investigated. The dye coded Z907 was employed as a sensitizer. The rheological properties and diffusion conductivity were determined to find an optimal gel that could be applied in a cell simply but did not affect much the diffusion conductivity. Then, the gel DSSC was fabricated and measured the solar cell performance compared to liquid one.

9.3 Experimental

9.3.1 Materials

70% purified Na-bentonite, natural clay (500 nm - 2 μm sizes) was kindly supplied from Thai Nippon Chemical Industry Co., Ltd, Thailand. Methyl acrylate monomer, ≥ 95% was from Merck, and Potassium peroxodisulphate, ≥ 98% was from Fluka. Z907 dye and materials (i.e. FTO glasses, TiO_2 electrode, and surlyne sheet) were supported from Laboratory of Photonics and Interfaces, EPFL. Liquid electrolyte was composed of 0.6 M BMII, 0.1 M I_2, 0.5 M TBP and 0.1 M GuNCS in MPN.

9.3.2 Polymethyl Acrylate Polymerization

0.58 M methyl acrylate monomer in 200 ml RO water was prepared and stirred under nitrogen atmosphere at 70 °C before adding 0.035 g of potassium peroxodisulphate (initiator) to start the soap-free polymerization. The reaction was controlled at the above condition for only 1 h to avoid aggregation of latex particles (Chen and Sajjadi, 2009).The dry weight of latex PMA as synthesized was 32.5 g/l.

9.3.3 Polymer/Clay Aerogel Preparation

Na-bentonite was purified further followed the technique described in Chapter VII and then 2g/l of purified Na-bentonite was swollen in RO water for overnight. Afterward, the PMA latex suspension from 9.3.2 was mixed with swollen purified Na-bentonite with the polymer: clay ratio of 100:0 defined as PMA100, 90:10 defined as PMA90, and 75:25 defined as PMA75 at 50°C for 1 hr. After cooled down, the PMA latex and 2 wt.% of mixtures were poured into Petri dishes, and then frozen at -80 °C before placed them in a freeze dryer (SCANVAC Coolsafe 110-4 pro) at temperature of -110 °C and pressure lower than 0.5 mbar for 24 hr. Then, dry composites were collected and kept in desiccators at room temperature before use.

9.3.4 Gel Electrolyte Preparation

The PMA/Na-bentonite aerogel was dried at 60 °C for 1 night. Then, liquid electrolyte was poured into the composite in a bottle and the mixture was left at room temperature for at least 1 h before homogenized the mixture by glass rod. Then, the ready used gel electrolytes were kept away from moisture in a tightly close bottle in desiccators.

9.3.5 Cell Assembly

The 9 μm-thick transparent TiO_2 films with active area of 0.283 cm^2 prepared in Laboratory of Photonics and Interfaces were immersed in 0.17 mM dye solution in 1:1 volume ratio of acetonitrile and *tert*-butanol. The counter electrode was prepared by dropped and wiped Pt solution of 10 mM chloroplatinic acid hydrate

in 2-propanol on FTO, TEC 15 and annealed at 400 °C for 15 min. Gel electrolyte was spread on a photoanode and then the cell was seal with a 25 μm-thick transparent surlyne ring from Dupont at 150 °C for 10 min. Liquid electrolyte was injected through a predrilled hole in the counter electrode after two electrode are sealed with melt-surlyne ring and then the hole was sealed with a surlyne sheet and a cover glass. Finally, double seal with Silicone and epoxy glue was applied on the gap between two electrodes of all cells.

9.3.6 Characterization and Measurement

9.3.6.1 Molecular Weight of Polymethyl Acrylate

The weight-average molecular weight (M_w) and number-average molecular weight (M_n) of PMA were obtained by SHIMADZU GPC-RID10A with refractive index detector. The Waters 600 controller chromatograph equipped with water Styragel HR 6E THF waters brand of 7.8mmID × 300 mm column was packed with high cross-links styrene divinylbenzene copolymer particle connected 3 columns (MW resolving range of 100-500,000). Tetrahydrofuran (THF), HPLC grade was used as an eluent. The operating condition was controlled at 40°C with flow rate 1.0 ml/min. Characteristics of the column were calibrated using narrow MWD polystyrene standard. 0.25% PMA was dissolved in THF before injected to GPC instrument.

9.3.6.2 FE-SEM Micrographs

The PMA latex was dropped on stuff and dried at room temperature. The composites were deposited on carbon-black taped on stuff and coated Pt by sputtering technique. A field emission scanning electron microscope (FE-SEM, Hitachi S4800) was utilized to observe the composite morphology. The V_{acc} and I_e were kept at 5.0 keV and 10 μA, respectively.

9.3.6.3 Rheological Properties

The Advanced Rheometric Expansion System (ARES) rheometer (Rheometrics Inc., Piscatway, NJ) with parallel-plate tool was utilized. The plate diameter was 25 mm. The gel was place on the bottom plate before the upper plate was lowered in to the gel. The excess material was trimmed off. The experiment was controlled at room temperature. The strain sweep was conducted at 1

frequency and %strain range of 0.1-15. The linear viscoelastic regime (LVR) of the sample was consequently used to choose %strain for frequency sweep. The frequency sweep was tested at frequency range of 0.1-100 rad/s with %strain in the field of linear viscoelasticity. The plots of elastic (G') and viscos (G") vs frequency were reported.

9.3.6.4 Diffusion Conductivities

The diffusion conductivity (σ_d) is a reciprocal of diffusion resistivity (ρ_d) and ρ_d is diffusion resistance (R_d) per unit area. The R_d was collected by fitting the impedance spectra of Nyquist plot and R_d was Z'_d-Z'_p at the phase is zero and at low frequency (~60 mHz). The impedance spectrum is shown in Fig. 9.1. The electrochemical impedance spectra were determined by a potentiostat/gulvanostat (μAutorlab type III/FRA 2). The gel is filled in between two Pt electrodes with 1cm^2 active area. The thickness of the gel was limited by 25 μm-thick surlyn spacer used for sealing the cell by heating. The silver paste was painted on the area for probe contacting to improve contact conductivity. The frequency was in the range of 0.5 MHz- 60 mHz. The amplitude was 0.3 V and the experiment was conducted at room temperature.

9.3.6.5 Photovoltaic Properties

The photovoltaic properties of the prepared DSSCs, i.e. short circuit current (J_{sc}, mA/cm^2), open circuit voltage (V_{oc}, V), fill factor (FF), and efficiency (η, %), were determined from the I–V curve obtained by using a digital Keithley model 2400 digital source meter (Keithley, USA) under an irradiation of a 450 W xenon light source (Oriel, USA) with an irradiance of 100 mWcm^{-2} (the equivalent of one sun at AM 1.5).

9.4 Results and Discussion

The M_w of PMA synthesized in this study was 598,685 and the M_n was 336,953. Meanwhile, The FE-SEM micrographs of PMA beads and PMA/Na-bentonite aerogel are shown in Fig. 9.2. The particle sized of PMA beads are found around 200 nm and most of them fused together and formed a flat film after water evaporation. Fig. 9.3 shows the general structure of clay aerogel (Bandi *et al.*, 2005;

Bandi and Schiraldi, 2006) with the bulk density of 0.02g/l and the Fig. 9.4, magnified image shows the PMA film coating on clay aerogel. Because PMA film is form a thin layer on clay surface instead of bulk PMA, there is the great number of open surface of PMA in composite and this enhances the rapidly contact between PMA and electrolyte during gel electrolyte preparation.

The plots of elastic (G') and viscos (G") vs frequency are shown in Fig. 9.5. The G' increased with composite content in liquid electrolyte and with clay content in composite. Since the gel point defined as the point that provides G' higher than G", the gel point of PMA100 starts at 25 wt.% composite while those of PMA90 and PMA75 start at 10 wt.% composite. This reveals that the incorporation of clay contributes the mixture to reach the gel point faster and provides the stronger and more stiffness gel. The stronger gel sometimes inverts to the slopes of the plot of G' and G" vs frequency, in addition G' and G" relatively more depend on frequency when their slopes are higher, and the stiffness directly depend on G'. These were mentioned in the study of Rosalina and Bhattacharya (2002). In fact, only PMA can gel MPN based-liquid electrolyte but Na-bentonite. Thus, in case PMA75 it needs more composite content in liquid electrolyte to obtain sufficient PMA to solidify liquid electrolyte while the gel simultaneously obtains stronger gel and more stiffness such that PMA75 render the highest G' compared at the same composite content (Fig. 9.5c). The G' of 30 wt.% PMA100 , 10 wt.% PMA90, and 10 wt.% PMA75 provide the slope of 0.6, 0.06, 0.1, respectively. The lower G' of 10 wt.% PMA75 compared to that of 10 wt.% PMA90 takes place from less PMA to absorb liquid electrolyte.

After the gel electrolytes were obtained, the conductivity of gel electrolyte is an important factor to be determined. Even though R_s (Fig.9.1) responding at high frequency (~ 40 kHz in this study) indicates to the ohmic serial resistance of the system and can be accounted for the resistance of the gel electrolyte (Longo *et al.*, 2002; Longo *et al.*, 2003), R_s mainly described the resistance of TCO (Hauch and Georg, 2001) and electrical contact, which is not properly controlled in this study due to the different shape of FTO glasses after cutting and thicknesses of silver paste for contact. Meanwhile, R_{ct} responding at medium frequency (~ 100 Hz) is the charge transfer resistance of Pt/electrolyte interface which are the sum of charge transfer resistance of cathode and anode (Hauch and Georg, 2001). It is hard to control the

amount of Pt coated on conducting glass by wiping technique since there are several factors influence to the homogeny of the film formation besides the concentration of Pt solution, such as rate of 2-propanol vaporization and hand force to wipe the solution on FTO glass. Last, the R_d, diffusion resistance responding to the diffusion of redox species in electrolyte (Hauch and Georg, 2001) at low frequency (~60 mHz). Therefore, the R_d would be the only characteristic of any gels. The diffusion conductivity of gels is shown in the Fig. 9.6. It was found that the σ_d decrease with increase of composite content in liquid electrolyte and with increase of clay content. Besides, this trend is in accordance with rheological properties.

Nevertheless, the weak gel with high diffusion conductivity is essential for good contact between dye and electrolyte since the weak gel can penetrate through the porous of semiconductor easily and quickly. The 10 wt.% PMA90 was the most possible since it provides the weak gel with the lowest G' and provides the best diffusion conductivity compared to the other composites at their gel points. The DSSC properties (J_{sc}, V_{oc}, *ff*, and $\%\eta$) of gel electrolyte are 7.80 mA/cm^2, 655 mV, 0.67, and 3.41%, and those of liquid electrolyte are 8.46 mA/cm^2, 725 mV, 0.63, and 3.89%. The semi-solid electrolyte diminishes the DSSC performance, namely the V_{oc} dropped by 70 mV, J_{sc} dropped by 0.66 mA/cm^2, and the conversion efficiency dropped by 0.48%. This is in agreement with the results from diffusion conductivity. Nevertheless, low diffusion conductivity should result in low current density and fill factor at the same time. However, fill factor of the cell with gel electrolyte is not deteriorated. Also, this could not be ascribed to high recombination rate which causes low V_{oc} and fill factor (Kalyanasundaram and Grätzel, 1998; Nazeeruddin *et al.*, 1993). Hence, the increasing of fill factor with decreasing of photocurrent of gel electrolyte implies that ion diffusion resistivity of gel electrolyte is not significantly high compared to that of liquid electrolyte and the diffusion conductivity of liquid electrolyte is 2.5 mS/cm, the same magnitude with that of gel electrolyte. Meanwhile, lower V_{oc} and J_{sc} is possibly a consequence of low contact between gel electrolyte and photoanode, as lower penetration of gel electrolyte compared to liquid one.

The improvement of J_{sc} is not found in this study. The macroscopic structure of Na-bentonite aerogel that collapses after liquid electrolyte exposure did

not only retard the ion diffusion and electron exchange pathway but also the penetration of gel electrolyte in mesoporous of TiO_2. Thus, the nanoscale exfoliated of clay in polymer gel electrolyte is the one possible to obtain the enhancement of the cell performance from purified Na-bentonite (Tu et al., 2008).

9.5 Conclusions

The composite of PMA/purified Na-bentonite was prepared to solidify liquid electrolyte. The optimal composite ratio and composite content in electrolyte was 10 wt.% PMA90, which gives the weak gel electrolyte and hence the highest diffusion conductivity of redox species. The DSSC conversion efficiency of gel electrolyte is 3.4%.

9.6 Acknowledgments

This work was financially funded by the Royal Golden Jubilee Ph.D. Program, Thailand; Rachadapiseksompote Endowment, Chulalongkorn University, Thailand; and National Nanotechnology Center, National Science and Technology Development Agency, Thailand. The authors would like to thank Thai Nippon Chemical Industry Co., Ltd for kindly providing the clay and thank Prof. Michael Grätzel, and his research associates, Dr. Shaik Mohammad Zakeeruddin, and Dr. Paul Liska from Laboratory for Photonics and Interfaces, Ecole polytechnique fédérale de Lausanne for the kindly providing all supports.

9.7 References

Bandi, S., and Schiraldi, D. A. (2006). Glass transition behavior of clay aerogel/poly(vinyl alcohol) composites. Macromolecules, 39(19), 6537-6545.

Berginc, M., Hočevar, M., Opara Krašovec, U., Hinsch, A., Sastrawan, R., and Topič, M. (2008). Ionic liquid-based electrolyte solidified SiO_2

nanoparticles dye-sensitized solar cells. Thin Solid Films, 516(14), 4645-4650.

Chen, Y., Sajjadi, S. (2009). Particle formation and growth in ab initio emulsifier-free emulsion polymerization under monomer-starved conditions. Polymer, 50(2), 357–365.

Kalyanasundaram, K., and Grätzel, M. (1998). Application of functionalized transition metal complexes in photonic and optoelectronic devices. Coordination Chemistry Reviews, 177(1), 347-414

Kay, A. (1994). Solar cell based on nanocrystalline TiO2 electrodes. Ph.D. Dissertation, Ecol Polytechnique fédérale de Lausanne (EPFL), Lausanne, Switzerland.

Lai, Y.-H., Chiu, C.-W., Chen, J.-G., Wang, C.-C., Lin, J.-J., Lin, K.-F., and Ho, K.-C. (2009). Enhancing the performance of dye-sensitized solar cells by incorporating nanosilicate platelets in gel electrolyte. Solar Energy Materials & Solar Cells, 93(10), 1860-1864.

Lai, Y.-H., Lin, C.-Y., Chen, J.-G., Wang, C.-C., Huang, K.-C., Liu, K.-Y., Lin, K.-F., Lin, J.-J., and Ho, K.-C. (2010). Enhancing the performance of dye-sensitized solar cells by incorporating nanomica in gel electrolytes. Solar Energy Materials & Solar Cells, 94(4), 668-674.

Longo, C., Nogueira, A. F., and De Paoli, Marco-A. (2002). Solid-state and flexible dye-sensitized TiO_2 solar cells: a study by electrochemical impedance spectroscopy. The Journal of Physical Chemistry B, 106(23), 5925-5930.

Longo, C., Freitas J., and De Paoli, Marco-A. (2003). Performance and stability of TiO_2/dye solar cells assembled with flexible electrodes and a polymer electrolyte. Journal of Photochemistry and Photobiology A: Chemistry, 159(1), 33–39.

Hauch, A. and Georg, A. (2001). Diffusion in the electrolyte and charge-transfer reaction at the platinum electrode in dye-sensitized solar cells. Electrochimica Acta, 46(22), 3457–3466.

Nazeeruddin, M.K., Kay, A., Rodicio, I., Humphry-Baker, R., Müller, E., Liska, P., Vlachopoulos, N., and Grätzel, M. (1993). Conversion of light to electricity by cis-X2bis(2,2'-bipyridyl-4,4'-dicarboxylate)ruthenium(II) charge-

transfer sensitizers (X = Cl-, Br-, I-, CN-, and SCN-) on nanocrystalline TiO2 electrodes. Journal of the American Chemical Society, 115(14), 6382-6390.

Rosalina, I., and Bhattacharya, M. (2002). Dynamic rheological measurements and analysis of starch gel. Carbohydrate Polymers, 48(2), 191-202.

Park, J. H., Kim, B.-W., and Moon, J. H. (2008). Dual functions of clay nanoparticles with high aspect ratio in dye-sensitized solar cells. Electrochemical and Solid-State Letters, 11(10), B171-B173.

Pojanavaraphan, T., Schiraldi , D. A., and Magaraphan, R. (2010). Mechanical, rheological, and swelling behavior of natural rubber/montmorillonite aerogels prepared by freeze-drying. Applied Clay Science, 50(2), 271–279.

Sasajima, K., Munakata, H., and Kanamura, K. (2008). Design of filling polymer electrolytes for 3DOM composite membrane. ESC Transactions, 16(2), 1443-1449.

Tu, C.-W., Liu, K.-Y., Chien, A.-T., Lee, C.-H., Ho, K.-C., and Lin, K.-F. (2008). Performance of gelled-type dye-sensitized solar cells associated with glass transition temperature of the gelatinizing polymers. European Polymer Journal, 44(3), 608–614.

Zakeeruddin, S.M., and Grätzel, M. (2009). Solvent-free ionic liquid electrolytes for mesoscopic dye-sensitized solar cell. Advanced Functional Materials, 19(14), 2187-2202.

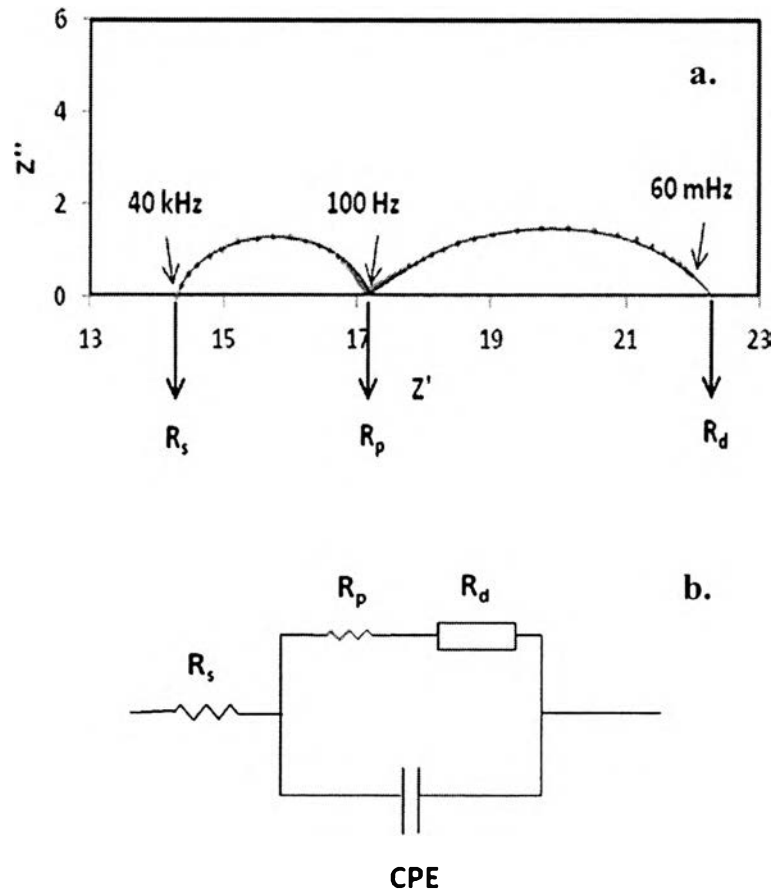

Figure 9.1 Nyquist diagram of the impedance spectra of 10 wt.% PMA90 gel electrolyte at amplitude of 0.3 V (a) and equivalent electrical circuit model of symmetric cell (b) (Pt//gel electrolyte//Pt), R_s is ohnic series resistance, R_p is charge transfer resistance (p = ct), R_d is diffusion resistance, and CPE is constant phase element.

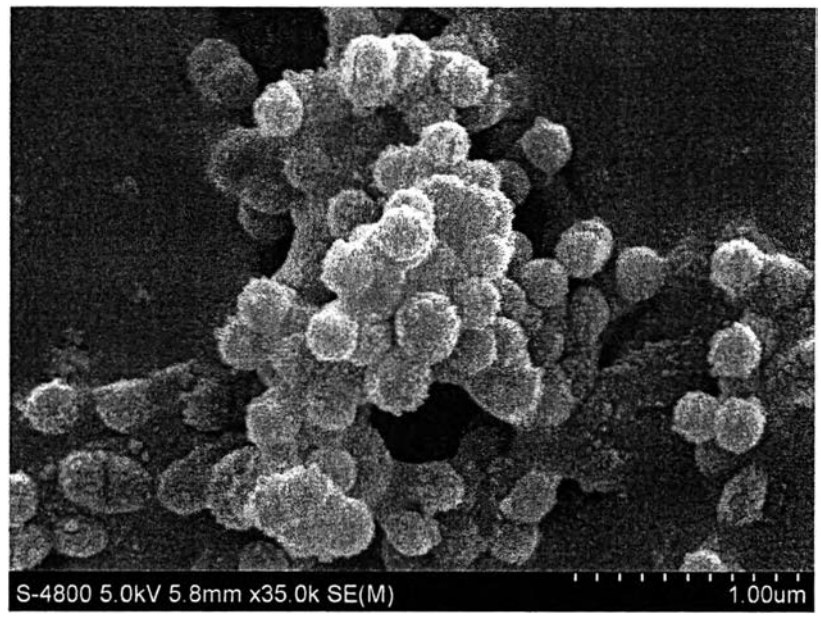

Figure 9.2 The FE-SEM micrograph of PMA beads.

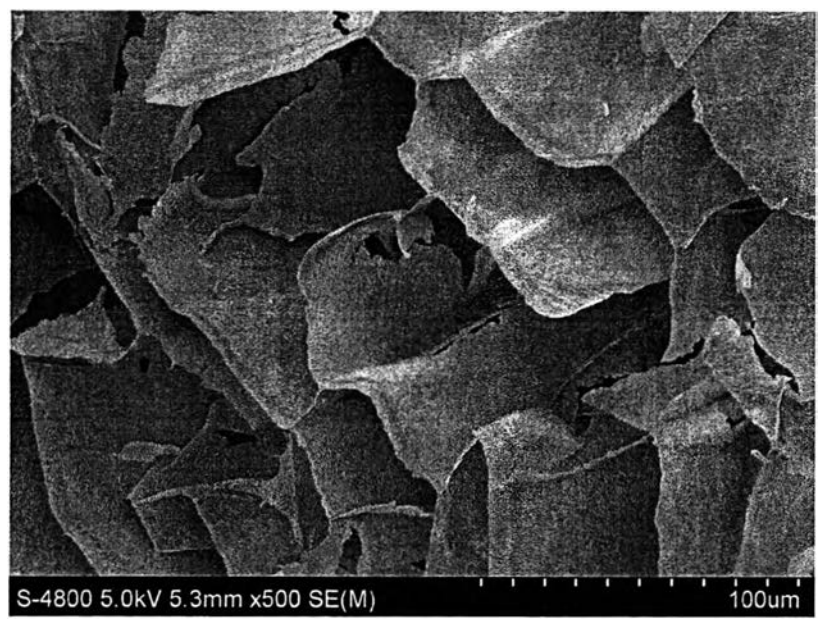

Figure 9.3 The FE-SEM micrograph of PMA/purified Na-bentonite aerogel.

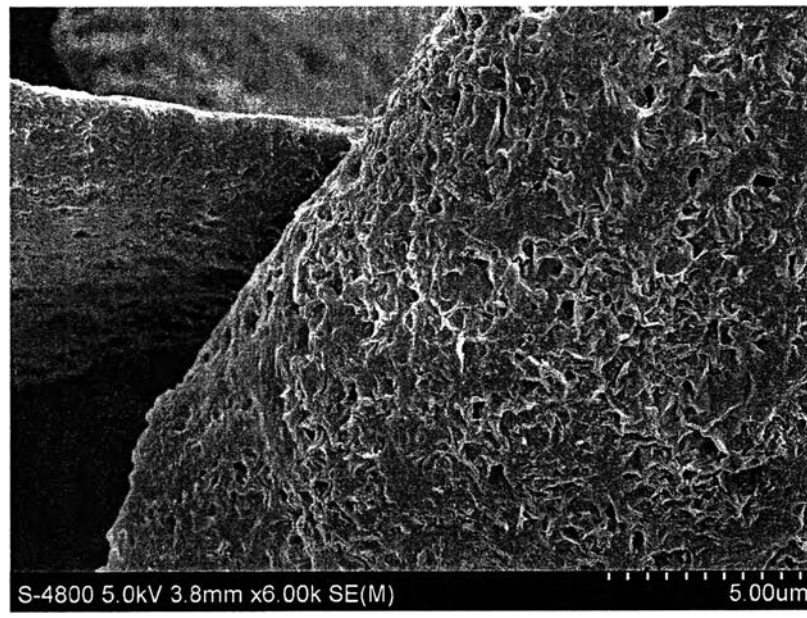

Figure 9.4 The FE-SEM micrograph of PMA film coating on clay aerogel.

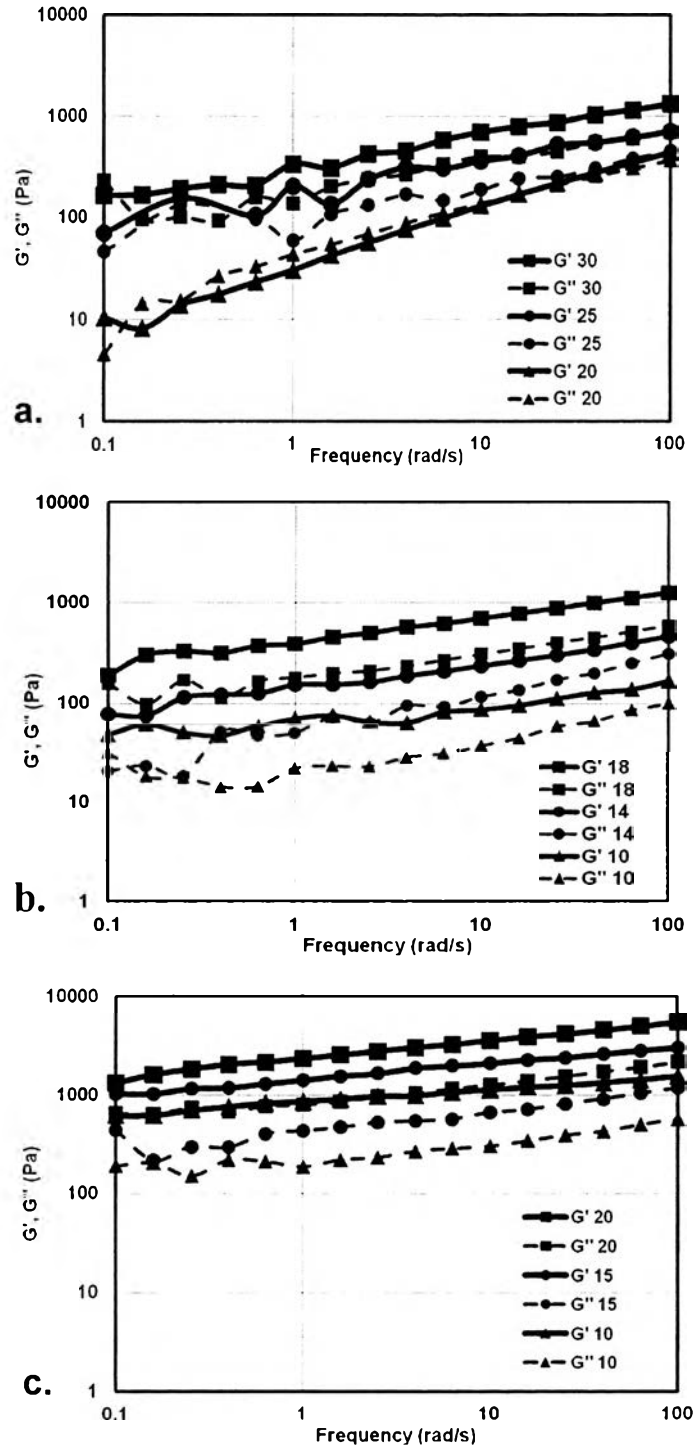

Figure 9.5 Dynamic frequency sweep data of (a) PMA100, (b) PMA90, (c) PMA75 at various contents in liquid electrolyte.

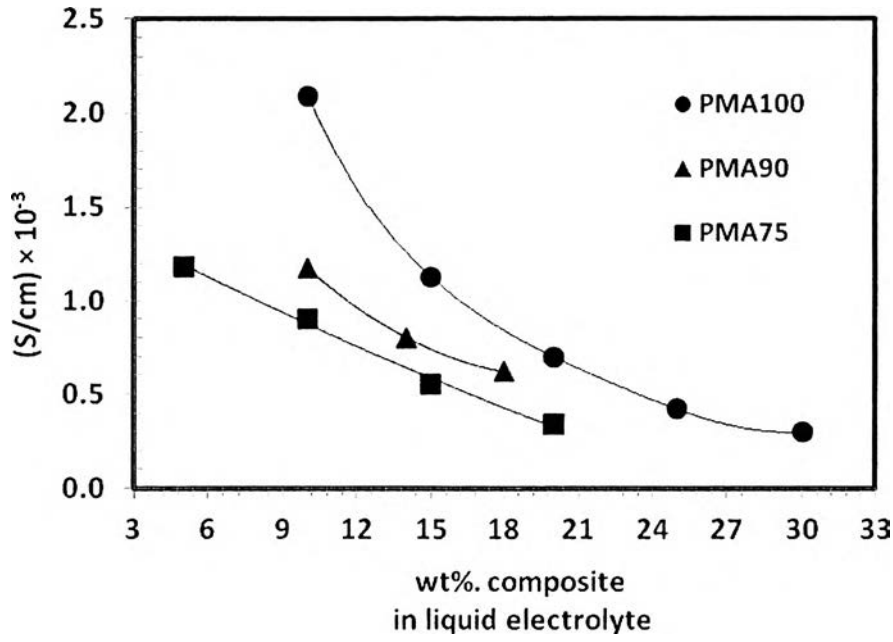

Figure 9.6 Diffusion conductivity of gel electrolytes at various composite content in liquid electrolyte.